Supporting Information

Dynamic plasticity and failure of microscale glass: Rate-dependent ductile-brittle-ductile transition

Rajaprakash Ramachandramoorthy[+1], Jakob Schwiedrzik[+1]*, Laszlo Petho[1], Carlos Guerra-Nuñez[1], Damian Frey[2], Jean-Marc Breguet[2], Johann Michler[1]**

[+] - Equal contribution

* - Corresponding authors

[1] - Laboratory of Mechanics of Materials and Nanostructures,

Empa – Swiss Federal Laboratories for Materials Science and Technology,

Feuerwerkerstrasse 39,

3602 – Thun. Switzerland.

[2] - Alemnis AG,

Feuerwerkerstrasse 39,

3602 – Thun. Switzerland.

Email: rajaprakash.ramachandramoorthy@empa.ch, jakob.schwiedrzik@empa.ch,

johann.michler@empa.ch

Supplementary Section S1: Literature survey of rate-dependent amorphous metallic glass testing

In amorphous metallic glass literature, a plethora of rate-dependent experimental [1, 2] and computational studies[3, 4] can be identified. The experimental studies are typically conducted using nanoindentation at different loading rates (typically 0.01mN/s – 300mN/s that translate to a strain rate of ~10^{-3}/s - 1/s),[5] though there are a few studies where uniaxial compression and tension has been used at displacement rates of 1-100nm/s.[6-8] The computational efforts have typically used kinetic monte-carlo simulations[9] and metadynamics[4, 10] for exploring the rate-effects in metallic glass. From these studies it can be understood that the plasticity in amorphous metallic glasses is dictated by the shear-band formation and this process is strain-rate and temperature dependent. A deformation map summarizing the typical behavior of metallic glasses show that at low strain rates (~<10^{-2}/s) and high temperature (~>0.8T_g, where T_g is the glass transition temperature) the deformation is homogeneous, at intermediate strain rates (~<0.1/s) and low temperature (~<0.7T_g) the deformation is serrated (inhomogeneous) and at high strain rates (~>1/s) the deformation is homogeneous again.[11, 12]

These experimental findings are corroborated by computational and analytical studies, and it is understood that at very low strain rates and high temperatures the thermally induced dispersion of shear transformation zones (STZ) throughout the bulk results in homogeneous or Newtonian viscous flow, at the intermediate strain rates the deformation is serrated due to the formation of discrete shear bands and at high strain rates the homogeneous flow has been hypothesized to be the simultaneous effect of multiple shear band activity.[1] Given these deformation mechanisms in amorphous materials are thermally activated, it can be intuitively understood that the strain rate at which these transitions in deformation mechanism occur are material and temperature dependent.[11] These peculiar transitions in deformation mechanisms were established previously in metallic glasses only using nanoindentation experiments, where the deformation volume continuously increases due to the triaxial stress state and hence interpreting the results is difficult.[13] This unfortunately led to multiple conclusions drawn for the reason behind these rate-dependent transitions in different studies, including machine compliance artifact and lack of instrument resolution.[1, 14] On the other hand, micropillar compression experiments typically possess a nearly uniaxial stress state and the results are easier to comprehend.[15] But so far due to lack of necessary instrumental capabilities, high strain rate experiments on micropillars beyond ~0.1/s have not been realized. Also, though several rate-dependent studies have been conducted on metallic glasses,[12, 16] there is a lack of such experiments on traditional amorphous glasses such as fused silica, borosilicate and soda-lime especially at the microscale. Recently, a computational study on the investigation of the avalanches during the deformation of amorphous micropillars, using metadynamics algorithm, showed that the microscale simulations can be conducted at strain rate ranges of 10^{-2}/s to 10^{6}/s,[4] but in order to validate such simulations, microscale high strain rate experiments are required.

Supplementary Figure S1: Comprehensive stress-strain curves obtained at different strain rates

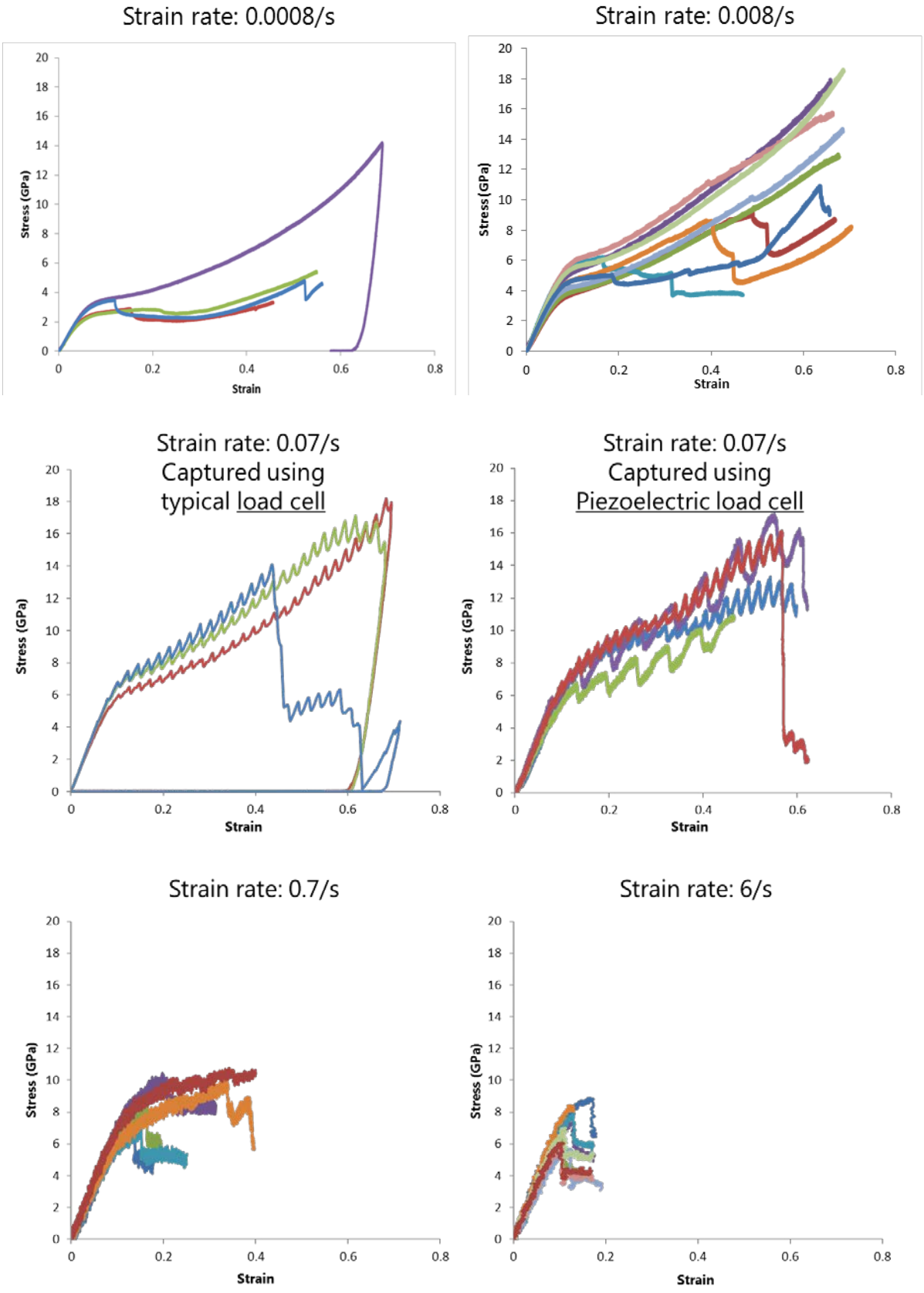

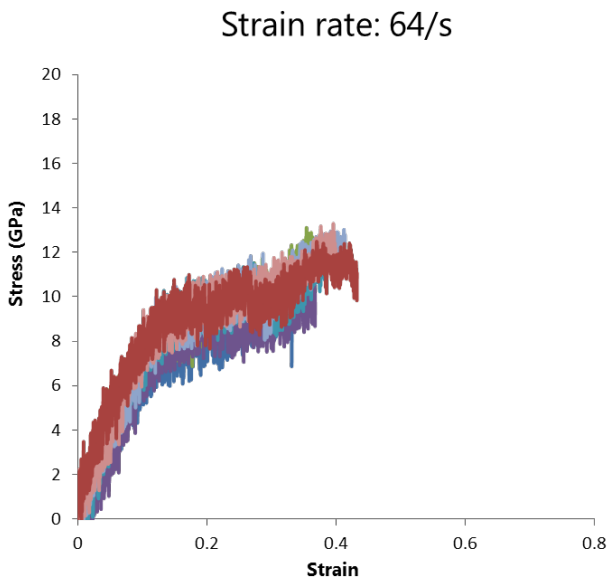
Strain rate: 64/s
Stress (GPa)
Strain
0
2
4
6
8
10
12
14
16
18
20
0
0.2
0.4
0.6
0.8

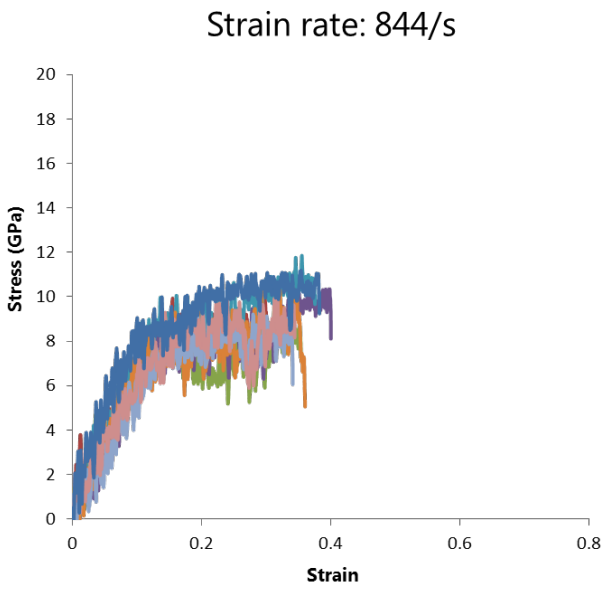
Strain rate: 844/s
Stress (GPa)
Strain
0
2
4
6
8
10
12
14
16
18
20
0
0.2
0.4
0.6
0.8

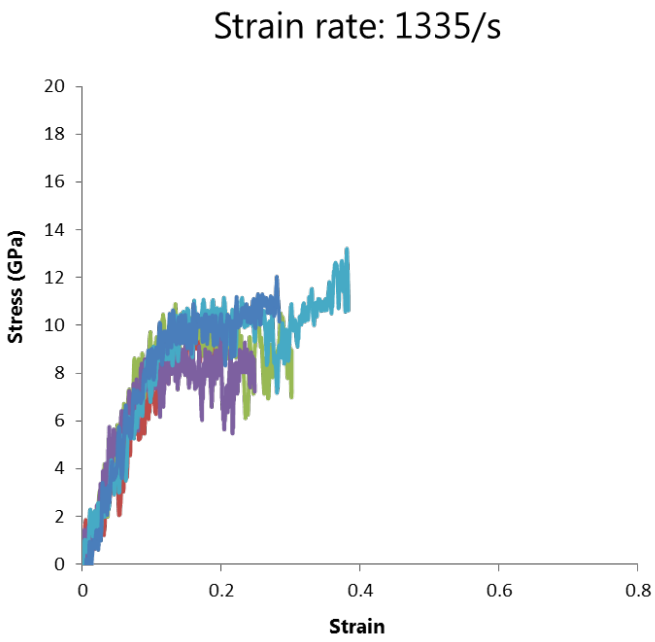
Strain rate: 1335/s
Stress (GPa)
Strain
0
2
4
6
8
10
12
14
16
18
20
0
0.2
0.4
0.6
0.8

Supplementary Figure S2: Schematic of the sequential shear band propagations

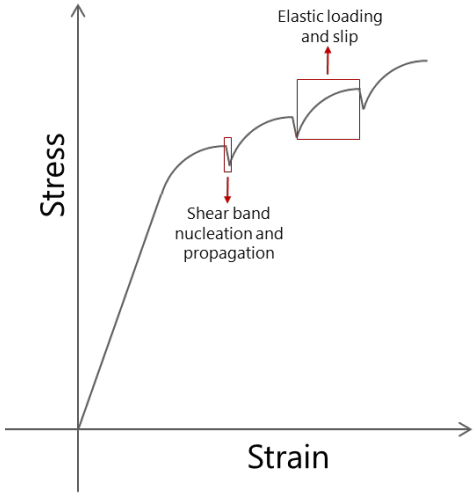

Supplementary table S1: Extracted parameters from stress-strain curves at different strain rates

Strain rate (/s)	Yield stress (GPa)	Taper corrected yield stress (GPa)	Elastic strain (µm/µm)	Plastic strain (µm/µm)	Failure strain (µm/µm)	Hardening modulus (GPa)	Taper corrected hardening modulus (GPa)
0.0008	1.20	0.99	0.05	1	1	4	-5.29
0.0008	1.62	1.34	0.06	1	1	4	-5.29
0.0008	2.08	1.72	0.03	1	1	6	-5.13
0.0008	2.44	2.02	0.03	1	1	8	-4.97
0.008	2.89	2.39	0.05	1	1	11	-4.73
0.008	2.94	2.43	0.05	1	1	8	-4.97
0.008	3.27	2.70	0.07	1	1	12	-4.65
0.008	3.37	2.79	0.07	1	1	10	-4.81
0.008	3.41	2.82	0.07	1	1	8	-4.97
0.008	3.39	2.80	0.07	1	1	8	-4.97
0.008	4.38	3.62	0.08	1	1	11	-4.76
0.008	4.51	3.73	0.08	1	1	8	-4.97
0.008	4.69	3.88	0.09	1	1	4	-5.29
0.07	5.20	4.30	0.07	1	1	17	-4.25
0.07	5.71	4.72	0.08	1	1	13	-4.57
0.07	5.70	4.71	0.08	0.55	0.63	10	-4.81
0.07	5.77	4.77	0.08	0.38	0.46	18	-4.17
0.07	5.30	4.38	0.08	0.54	0.61	16	-4.33
0.07	5.65	4.67	0.07	0.55	0.62	8	-4.97
0.07	6.23	5.15	0.08	0.51	0.59	14	-4.49
0.7	6.00	4.96	0.09	0.31	0.40	16	-4.33
0.7	5.44	4.50	0.09	0.15	0.24	16	-4.33
0.7	7.34	6.07	0.10	0.29	0.39	22	-3.85
0.7	7.29	6.02	0.11	0.20	0.31	40	-2.42
0.7	7.00	5.79	0.10	0.09	0.19	30	-3.21

0.7	5.70	4.71	0.10	0.07	0.17	27	-3.45
6	6.37	5.26	0.10	0.06	0.16	N/A	N/A
6	6.02	4.98	0.10	0.07	0.17	N/A	N/A
6	7.00	5.78	0.09	0.07	0.16	N/A	N/A
6	7.41	6.12	0.09	0.10	0.19	N/A	N/A
6	5.09	4.21	0.09	0.07	0.16	N/A	N/A
6	5.65	4.67	0.12	0.05	0.17	N/A	N/A
6	6.15	5.08	0.11	0.06	0.17	N/A	N/A
6	5.94	4.91	0.12	0.06	0.18	N/A	N/A
64	7.83	6.47	0.14	0.29	0.43	2.00	-5.45
64	7.93	6.55	0.13	0.26	0.39	5.00	-5.21
64	7.50	6.20	0.13	0.28	0.41	9.00	-4.89
64	7.45	6.16	0.12	0.25	0.37	9.00	-4.89
64	8.06	6.66	0.12	0.24	0.36	9.00	-4.89
64	8.12	6.71	0.11	0.25	0.36	15.00	-4.41
64	8.29	6.85	0.13	0.20	0.33	9.00	-4.89
844	8.39	6.93	0.14	0.16	0.30	20.00	-4.01
844	7.48	6.18	0.14	0.20	0.34	2.00	-5.45
844	8.20	6.78	0.14	0.20	0.34	2.00	-5.45
844	7.57	6.26	0.13	0.22	0.35	2.00	-5.45
844	8.10	6.69	0.11	0.25	0.36	2.00	-5.45
844	7.68	6.35	0.12	0.28	0.40	5.00	-5.21
844	8.50	7.02	0.13	0.24	0.37	-5.00	-6.01
1335	8.80	7.27	0.13	0.25	0.38	-8.00	-6.24
1335	9.10	7.52	0.13	0.07	0.20	-4.00	-5.93
1335	8.23	6.80	0.11	0.17	0.28	-2.00	-5.77
1335	9.65	7.98	0.10	0.15	0.25	-7.00	-6.16
1335	8.70	7.19	0.11	0.19	0.30	-13.00	-6.64

Supplementary table S2: Shear band propagation speed (=Displacement due to strain burst (mm) / time for strain burst(s)) for the different experiments in the Serrated strain rate regime.

Strain rate (/s)	Average shear band displacement for strain burst (nm)	Average time taken for strain burst (s)	Speed of shear band propagation (mm/s)	Average Displacement accommodated between stress drops (nm)
6	237.18	0.00048	0.4941	-
6	148.65	0.00046	0.3231	-
6	165.04	0.00042	0.3930	-
6	172.69	0.00052	0.3321	-
6	256.85	0.00062	0.4143	-
6	226.25	0.00066	0.3428	-
6	179.25	0.00074	0.2422	-
6	225.15	0.0008	0.2814	-
0.7	182.53	0.0043	0.0424	364.69

0.7	212.04	0.0045	0.0471	428.45
0.7	43.72	0.0082	0.0053	-
0.7	174.88	0.0054	0.0324	765.08
0.7	182.53	0.013	0.0140	-
0.7	47.00	0.0076	0.0062	-
0.07	88.67	0.0608	0.0015	434.57
0.07	157.83	0.11024	0.0014	119.35
0.07	182.80	0.12825	0.0014	403.96
0.07	110.06	0.0652	0.0017	112.47
0.07	126.46	0.065	0.0019	126.24
0.07	120.66	0.0653	0.0018	120.12
0.07	122.75	0.0657	0.0019	120.88

Supplementary Section S2: FEM modeling to correct for taper

A mesh refinement study showed that the mesh had converged to a stable solution with changes in yield stress <0.5% and in hardening slope <2.5% for a change in mesh density by a factor of 2. In a second step, the influence of surface cracking on the measured force-displacement curve was assessed. In order to do this, the model was enriched using XFEM and a maximum tensile stress criterion (s_{max}=0.75GPa) was used to allow crack formation in the model without preselection of the potential crack sites. It was found that indeed surface cracks formed in the axial-radial plane in the top portion of the pillar due to tensile hoop stresses. However, no significant load drops were observed in the FE simulations. It was found that the influence of the surface cracks was <2% for both yield stress and hardening modulus. Therefore, the following simulations were performed without consideration of surface cracking.

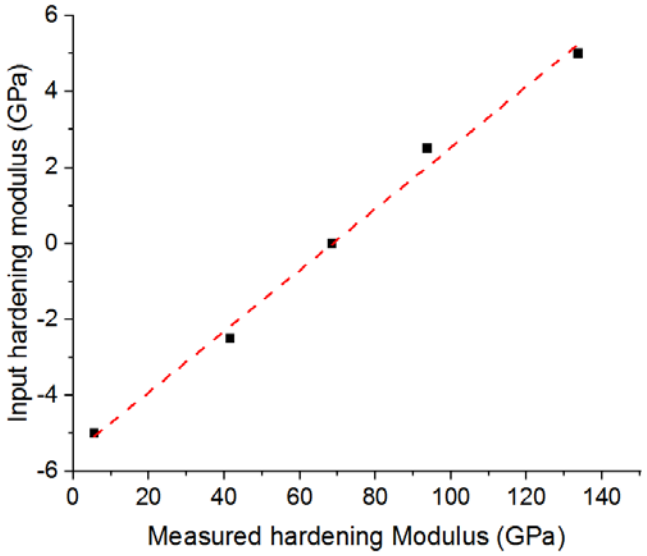

Figure S3: Material hardening slope as a function of the experimentally obtained hardening exponent

Lastly, it was checked whether the cap allowing volumetric plastic deformation has a significant influence on the mechanical behavior of the tapered micropillars. Therefore, the cap plasticity model was compared to a perfect J2 plasticity featuring the same uniaxial flow stress. It was found that the

yield stress is increased by 2.5%, while the hardening modulus decreased by 0.7% when using the von Mises model. It therefore seems that volumetric plastic deformation plays only a minor role in micropillar compression of fused silica at strains <20%.

In order to unambiguously understand the influence of taper on the absolute stress-strain values, FEM simulations were conducted to compare the apparent engineering stress-strain curves of tapered pillars with non-tapered pillars. It was found that the loading modulus of the tapered pillars is overestimated by a factor of 1.99, the yield stress by a factor of 1.21 compared to a perfect geometry. Subsequently, the influence of the material hardening on the experimentally measured hardening modulus was assessed. For this, linear isotropic hardening or softening of the J2 plasticity was introduced and the hardening slope $H = \frac{d\sigma}{d\varepsilon_p}$ varied from -5GPa to 5GPa in steps of 2.5GPa. Figure S3 shows the material hardening slopes of the J2 plasticity as a function of the experimentally obtained hardening slope of the tapered pillars. It was found that the resulting apparent hardening slopes (H_{exp}) of the tapered pillars follow a linear relationship with the actual material hardening (R^2=0.997), which allows estimating the material hardening slope (H_{mat}) from the experimental data using Equation 1.

$$H_{mat} = \frac{H_{exp} - 70.314}{12.541} \quad (1)$$

with H_{mat}, H_{exp} in GPa. Furthermore, it was verified that there was no significant influence ($p<0.05$) of the material hardening slope on the measured yield point and the variations remained very small (<1.5%). Next, the influence of potential misalignment between sample and flat punch indenter was assessed. It was found that a misalignment of 1°, which is a realistic value for *in situ* micromechanical testing, results in an overestimation of 4% in yield stress and an underestimation of 2.5% in hardening.

Supplementary Section S3: Effects of electron beam radiation

The fused silica micropillars were imaged using an SEM at 10kV and 10pA, for alignment of the pillars under the indenter tip and were also subsequently imaged during the tests. There are previous studies on amorphous silica nanobeads and nanowires (~20-500nm diameter) that show that the mechanical properties can be affected by intense TEM radiation at 200keV.[17, 18] But given that the electron beam current density is smaller in an SEM and the amorphous silica micropillars are significantly larger compared to the nanoscale beads used in previous studies, we hypothesized that the mechanical properties are not affected by the electron beam irradiation. Subsequently, we also performed tests with and without electron beam exposure and we did not see any significant change in the mechanical properties, as shown in the stress-strain curves showed in Figure S2. Also, in previous studies, by Kermouche et al, the yield stress-levels obtained for amorphous micropillars at a strain rate of ~0.02/s is ~6GPa.[19] This value matches with the yield stress obtained in our current study at strain rate of ~0.07/s as seen from Figure S4.

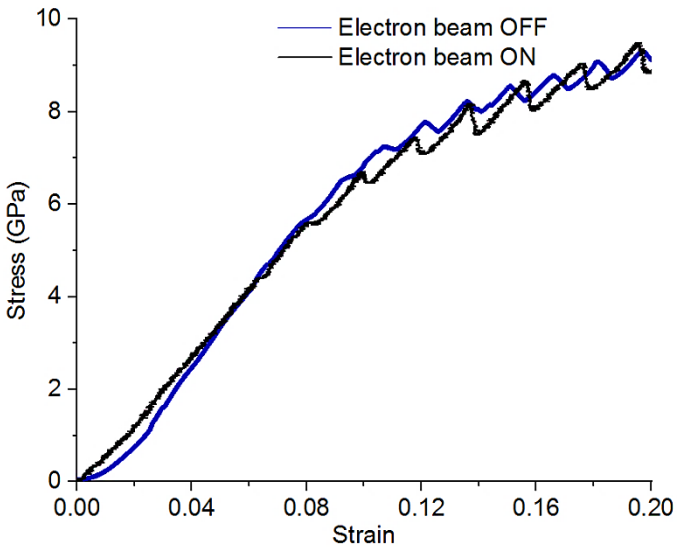

Figure S4: Stress-strain curves of amorphous fused silica with and without electron beam.

We also conducted comparative RAMAN studies between undeformed amorphous silica micropillars that are non-irradiated and electron beam irradiated at 10kV, 10pA for 10min. As seen from Figure S5, we cannot see significant differences between the two cases, specifically we do not observe peak sharpening/broadening or peak shifting due to electron beam creation of structural and bonding defects or induced densification respectively.[20, 21]

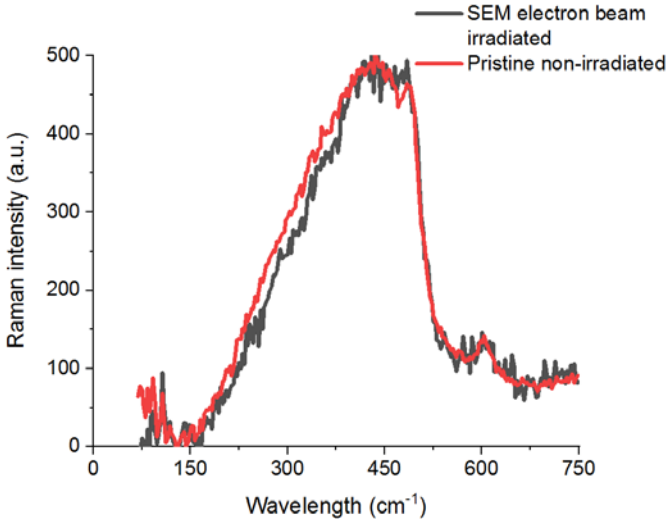

Figure S5: Comparison of RAMAN spectra obtained from an irradiated and non-irradiated amorphous silica micropillar

A recent study by Mačković et al on the irradiation effects of intense TEM electron beam on silica membranes showed that even at high current densities no marked structural change can be identified via RAMAN spectra in silica.[22] They hypothesized that the mechanical property differences noticed when the tests were conducted with the TEM electron beam ON could be due to local heating of the sample from the intense electron beam. In this current study, given that the current densities are much lower in the SEM, we can again neglect the effect of heating due to electron beam.

Supplementary Section S4: Statistical Analysis

Since multiple micropillars (4 – 9 pillars each: please refer to Supplementary table T1) were tested at each strain rate, a multivariate regression analysis was conducted to understand the statistical significance. In a multivariate regression, we are trying to asses if the predictor (strain rate) is jointly contributing to a number of different response variables (yield stress and plastic strain). Thus in our case, strain rate was taken as the independent variable and the yield stress and plastic strain extracted from every experiment were taken as the two dependent variables. Using R software for the regression analysis, we obtained a p value of 9.27e-7 and 0.0068 for yield stress and plastic strain respectively. Since the p value is <0.05, we can conclude that the changes in yield stress and plastic strain across experiments are specifically due to the changes in strain rate and this dependence is indeed statistically significant. It should also be noted that from the sign of the regression line's slope, it was determined that the yield stress has an increasing trend (slope: 0.002773) and the plastic strain has a decreasing trend (slope: -2.723e-4) with strain rate.

References

1. Schuh, C. A.; Lund, A. C.; Nieh, T. *Acta Materialia* **2004,** 52, 5879-5891.
2. Schuh, C.; Nieh, T.; Kawamura, Y. *Journal of Materials Research* **2002,** 17, 1651-1654.
3. Harris, M. B.; Watts, L. S.; Homer, E. R. *Acta Materialia* **2016,** 111, 273-282.
4. Cao, P.; Dahmen, K. A.; Kushima, A.; Wright, W. J.; Park, H. S.; Short, M. P.; Yip, S. *Journal of the Mechanics and Physics of Solids* **2018,** 114, 158-171.
5. Yang, B.; Nieh, T. *Acta Materialia* **2007,** 55, 295-300.
6. Kimura, H.; Masumoto, T. *Acta Metallurgica* **1983,** 31, 231-240.
7. Dubach, A.; Raghavan, R.; Löffler, J. F.; Michler, J.; Ramamurty, U. *Scripta Materialia* **2009,** 60, 567-570.
8. Mukai, T.; Nieh, T.; Kawamura, Y.; Inoue, A.; Higashi, K. *Scripta materialia* **2002,** 46, 43-47.
9. Homer, E. R.; Schuh, C. A. *Acta Materialia* **2009,** 57, 2823-2833.
10. Rodney, D.; Tanguy, A.; Vandembroucq, D. *Modelling and Simulation in Materials Science and Engineering* **2011,** 19, 083001.
11. Schuh, C. A.; Hufnagel, T. C.; Ramamurty, U. *Acta Materialia* **2007,** 55, 4067-4109.
12. Schuh, C.; Nieh, T. *Acta Materialia* **2003,** 51, 87-99.
13. Lacroix, R.; Kermouche, G.; Teisseire, J.; Barthel, E. *Acta Materialia* **2012,** 60, 5555-5566.
14. Jiang, W.; Atzmon, M. *Journal of materials research* **2003,** 18, 755-757.
15. Maeder, X.; Mook, W.; Niederberger, C.; Michler, J. *Philosophical Magazine* **2011,** 91, 1097-1107.
16. Nieh, T.; Schuh, C.; Wadsworth, J.; Li, Y. *Intermetallics* **2002,** 10, 1177-1182.
17. Zheng, K.; Wang, C.; Cheng, Y.-Q.; Yue, Y.; Han, X.; Zhang, Z.; Shan, Z.; Mao, S. X.; Ye, M.; Yin, Y. *Nature communications* **2010,** 1, 24.
18. Mačković, M.; Niekiel, F.; Wondraczek, L.; Spiecker, E. *Acta Materialia* **2014,** 79, 363-373.
19. Kermouche, G.; Guillonneau, G.; Michler, J.; Teisseire, J.; Barthel, E. *Acta Materialia* **2016,** 114, 146-153.
20. Kim, C.; Lim, S.; Jeong, C. *Journal of the Korean Physical Society* **2014,** 64, 1091-1095.
21. Saavedra, R.; León, M.; Martín, P.; Jimenez-Rey, D.; Vila, R.; Girard, S.; Boukenter, A.; Ouerdane, Y. In *Raman measurements in silica glasses irradiated with energetic ions*, AIP Conference Proceedings, 2014; AIP: pp 118-124.
22. Mačković, M.; Przybilla, T.; Dieker, C.; Herre, P.; Romeis, S.; Stara, H.; Schrenker, N.; Peukert, W.; Spiecker, E. *Frontiers in Materials* **2017,** 4, 10.